Int. J. Nanoelectronics and Materials **3** (2010) 23-36

Magnetic and electrical behaviour of $La_{0.67}Ba_{0.33}Mn_{1-x}Fex_{O3}$ perovskites

M. Baazaoui[1], S. Zemni[1*], M. Boudard[2,3], H. Rahmouni[4], A. Gasmi[1,2], A. Selmi[5], M. Oumezzine[1]

[1]Laboratoire de Physico–Chimie des Matériaux, Faculté des Sciences de Monastir, Département de Physique, 5019, Monastir, Tunisie.
[2]Laboratoire des Matériaux et du Génie Physique (CNRS UMR 5628), Minatec Bâtiment INPG, parvis Louis Néel, BP 257, 38016 Grenoble Cedex 1, France.
[3] SIMAP/ENSEEG, UMR5614 CNRS/INPG /UJF, BP75, 38402 St Martin d'Heres Cedex, France.
[4]Laboratoire de Physique des matériaux et nanomatériaux appliqués à l'environnement, Faculté des Sciences de Gabes, Département de Physique,6079 Gabes, Tunisie.
[5] Laboratoire de Physique des Semiconducteurs et des Composants Electroniques, Faculté des Sciences de Monastir, Département de Physique, 5019, Monastir, Tunisie.

Abstract

We have investigated the effect of Fe^{3+} substitution on electrical and magnetic properties of $La_{0.67}Ba_{0.33}Mn_{1-x}Fe_xO_3$ ($0 \leq x \leq 0.2$) manganese perovskites. Polycrystalline samples were prepared by the conventional ceramic method at 1180°C. Grain size and phase identification of specimens were carried out by X-ray diffraction techniques and morphological analysis by scanning electron microscope (SEM). The structure refinement by the Rietveld method revealed that all the compounds are a single phase manganite crystallizing in a rhombohedral ($R\bar{3}c$) perovskite structure. Magnetization as a function of temperature, M (T) in zero field cooled (ZFC) mode, shows a paramagnetic (PM) to ferromagnetic (FM) phase transition below 10% iron concentration and a spin glass-behaviour above. Magnetization as a function of magnetic field measurement at 10K shows that below 10% Fe^{3+} doping, the materials exhibit a strong ferromagnetic behaviour, while above that

[*]) For correspondence; Email: zemnis@yahoo.fr.

concentration; aantiferromagnetic behaviour is predominant for specimens. Electrical-resistivity measurement in the temperature range 80 - 320K shows metal – semiconductor transition at peak temperature T_P below 10% Fe^{3+} ion doping with a decrease in T_P and an increase in the maximum of resistivity (ρ_{max}). Above 10% Fe^{3+} amount the materials exhibit only a semiconductor-like behaviour. Interestingly, with the increase in doping concentration, T_C and T_P follow the same trend indicating coupling of electric and magnetic properties. Changes in these properties have been analysed on the basis that the substitution of Fe^{3+} for Mn^{3+} reduces the number of available hopping sites for the Mn $e_g(\uparrow)$ electron and suppresses the double exchange (DE), rather than lattice effect which is insignificant due to similar ionic radii of Fe^{3+} and Mn^{3+}.

Keywords: Iron doping rate, X-ray diffraction; Magnetic and electrical properties.
PACS: 76.30.Fc, 78.70.Ck, 73.61.-r.

1. Introduction

Recent observations of the colossal magnetoresistance (CMR) and other intricate physical properties in perovskite manganese oxides $R_{1-x}A_xMnO_3$ (R- trivalent rare earth, A – bivalent ion) have triggered renewed attention to this class of materials [1-4]. The manifestation of CMR around the paramagnetic to ferromagnetic transition temperature (T_C) is the generic feature of the systems with x~ 0.3. In order to explain such behaviour, the double exchange (DE) model was initially proposed [5-7]. However, the recent study [8] has pointed out that DE alone cannot explain the CMR behaviour of the manganites oxides and a strong Jhan-Teller effect (the strong electron-phonon interaction) also plays an important role in CMR. As is well known, $LaMnO_3$ has basically an antiferromagnetic insulator (AFI) characterized by a super exchange (SE) coupling between Mn^{3+} ions. By changing the oxygen stoichiometry or by substituting a divalent cation (A^{2+}) in place of La^{3+} a percentage of Mn^{4+} ions appears and $LaMnO_3$ can be driven into a metallic state, meanwhile, it exhibits a ferromagnetic ground state, which was ascribed to DE between Mn ions in Mn^{3+}-O-Mn^{4+} couples. As the nearest-neighbouring compound of $LaMnO_3$, the perovskite iron oxide

$LaFeO_3$ has similar magnetic and transport properties, i.e., insulating and antiferromagnetic, however the hole-doped $La_{1-x}A_xFeO_3$ continues to have an antiferromagnetic ground state and remains insulating even at the maximum extent of hole - doping [9]. It is worth pointing out that Mn^{3+} and Fe^{3+} have almost identical ion size [10]. In the last few years, extensive studies have been carried out by doping at Mn- site by various researchers [11-17]. They have suggested that Mn-site doping hampers the DE mechanism forcing the change in magnetic properties and influences the polaronic transport which causes change in polaron hoping distance and also the polaron concentration. Most of the studies on the Fe-substituted-lanthanum manganites have been focused on $La_{1-x}Sr_xMnO_3$ [18-21] and $La_{1-x}Ca_xMnO_3$ [22-25] systems. Contrarily the Fe-doped $La_{1-x}Ba_xMnO_3$ system is much less investigated though it was the material of the initial discovery of the CMR effect in the form of thin films [1]. Previously low percentage doping of Fe ($x \leq 0.1$) in $La_{0.67}Ba_{0.33}Mn_{1-x}Fe_xO_3$ manganites has been studied [11]. In order to more investigate structural, magnetic and electrical properties, especially to determine the limiting value of Fe doping, which eliminates the metal-semiconductor (MS) transition, we have attempted to study the substitution of higher concentration of Fe at Mn-site in $La_{0.67}Ba_{0.33}Mn_{1-x}Fe_xO_3$ ($0 \leq x \leq 0.2$). Fe was chosen as the dopant because the ionic radii of Mn^{3+} and Fe^{3+} are close to each other, so it is expected that the crystalline structure remains almost not modified by Fe substitution. Consequently lattice effects may be ignored and effects due to the variation in electronic structure become accessible. Fe may therefore be used as a control parameter to vary the magnetic and transport properties of these manganites.

2. Experimental

Perovskite manganese oxides with nominal composition $La_{0.67}Ba_{0.33}Mn_{1-x}Fe_xO_3$ ($0 \leq x \leq 0.2$) were prepared by standard ceramic solid state reaction at 1180°C. The microstructure was observed by scanning electron microscope (SEM). Powder X-ray diffraction (XRD) patterns were carried out with a ‘’PANalytical X’Pert Pro’’ diffractometer with filtered (Fe-filter) Co radiation. Data for the Rietveld refinement were collected in the 2θ range 10° - 100° with a step size of 0.017° and a counting time of 18 s per step. The

structure refinement was carried out by the Rietveld analysis of the powder XRD data with the FULLPROF software [26]. The temperature dependence of the magnetization, M (T), was measured under a constant magnetic field (0.05 T) with ZFC mode in the 10-400K and 10-300K temperature ranges, respectively for non doped compound (x=0) and doped compounds (x=0.05 - 0.2) using a linear extracting magnetometer equipped with a superconducting coil. On the same apparatus, the magnetization as a function of magnetic field M (H) measurements were carried out at 10K in the 0 - 10 T magnetic field range. Resistivity of the samples was measured with the conventional four probe method in the 80-320 K and in 80-300 K temperature ranges, respectively for non doped compound and doped compounds.

3. Results and discussion

3.1 Structural properties

Fig. 1 exemplifies the XRD patterns for x = 0 and x = 0.15 compounds. All $La_{0.67}Ba_{0.33}Mn_{1-x}Fe_xO_3$ samples show single phase character where the hexagonal setting in rhombohedral $R\bar{3}c$ symmetry is used for indices of diffraction lines of the manganites. The position of the most intense peak (lower inset of Fig. 1) has a negligible shift with varying Fe composition, indicating that the cell volume of $La_{0.67}Ba_{0.33}Mn_{1-x}Fe_xO_3$ specimens should be not affected by Fe doping. This inset shows also a little increase in peak broadening as a function of Fe amount, which may not considerably affect the grain size in these manganites.

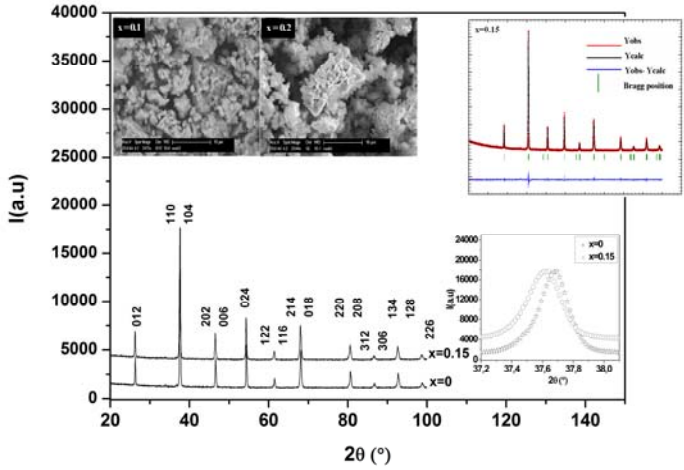

Fig.1: Powder XRD pattern for x = 0 an 0.15 $La_{0.67}Ba_{0.33}Mn_{1-x}Fe_xO_3$ compounds at room temperature. Indexing of the rhombohedral manganites corresponds to the hexagonal setting. The lower inset shows X- ray diffraction profiles for the most intense peak. The observed and calculated XRD patterns obtained by Rietveld analysis for x = 0.15 specimen is shown in the right upper inset. The upper left inset represents SEM micrographs for x=0.1 and 0.2 compositions.

The average crystallites sizes were calculated using the XRD data applying Rietveld refinement formula

$$G_S = \frac{180\lambda}{\pi\sqrt{IG}} \qquad (1)$$

where λ is the X-ray wave length and IG is the Gaussian size parameter given by Rietveld refinement. As it can be seen in table 1, the size of the crystallites is estimated to be between 40 and 50 nm when Fe amount varies between 5% and x = 20%, and hence no noticeable size effect was introduced by Fe doping. SEM micrographs (left inset of Fig 1) show that the samples are constituted of homogenous particles, ranging in size between 0.5 and 5μm and all compounds present an almost equal average grain size, significantly bigger than the values determined by XRD. This is because observations by imaging techniques such as SEM often give the size

of the secondary particles, and the X-ray line broadening analysis disclosed the size of primary particles. Rietveld structure refinement was performed in the hexagonal setting of the rhombohedral $R\bar{3}c$ space group (number 167), in which the (La, Ba) atoms are at 6a (0, 0, 1/4) position, (Mn, Fe) at 6b (0, 0, 0) and O at 18e (x, 0, ¼). A typical example of the observed and calculated diffraction profiles of the sample with x = 0.15 is shown in the right upper inset of Fig. 1. Detailed results of this refinement are listed in table I.

Table 1: Room-temperature structural parameters (Rietveld refinement) for the rhombohedral $R\bar{3}c$ phase $La_{0.67}Ba_{0.33}Mn_{1-x}Fe_xO_3$ ($0 \le x \le 0.2$); W is the band width, G_S is the estimated average grain size; R_{wp}, R_p and R_F are the residuals for respectively the weighted pattern, the pattern and the structure factor; χ^2 is the goodness of fit. The numbers in parentheses are estimated standard deviations to the last significant digit.

x		0	0.05	0.1	0.15	0.2
$R\bar{3}c$ phase						
a (nm)		0.55191(3)	0.55353(2)	0.55350(4)	0.55258(2)	0.55291(1)
c (nm)		1.35509(9)	1.35240(8)	1.3520 (1)	1.35724(7)	1.35869(6)
V (nm^3)		0.35752(3)	0.35886(3)	0.35872(5)	0.3589(3)	0.35971(2)
(La/Ba)	B_{iso} (nm^2)	0.00036(5)	0.00531(0)	0.002(0)	0.001(0)	0.0019 (3)
(Mn)	B_{iso} (nm^2)	0.00298(71)		0.002(0)	0.0099(6)	0.0097(5)
(O)	x	0.00609(0)		0. 525(2)	0.538(2)	0.467(2)
	B_{iso} (nm^2)	0.512 (2)	0. 529 (1)	0.01614(0)	0.00803(18)	0.00860(13)
$d_{(Mn,Fe)-O}$ (nm)		0.0101(14)				
$\Theta_{(Mn,Fe)-O-(Mn,Fe)}$(°)		0.00870(0)				
W(a.u)				0.1960(7)	0.1966(1)	0.1965(1)
G_S (nm)		0.1953(2)		171.90(3)	167.74(5)	169.44(4)
		176.27(3)	0.1962(6)	299	295	296
		170.52(3)		55	50	43
		303				
		61				
			298			
			41			
R_{wp} (%)		3.11	2.62	2.78	3.01	2.40
R_p (%)		2.35	2.03	2.15	2.33	1.83
R_F (%)		2.54	2.23	2.96	3.49	1.56
χ^2 (%)		1.36	1.02	1.08	1.17	1.58

We can see from the results indicated in table I that the cell volume is slightly varying between 0.35886(3) nm^3 for x=0.05 and 0.35971(2) nm^3 for x=0.2, so no noticeable structural change by Fe doping can be identified. According to Jonker and Ahn et al. [27, 28] iron enters into samples as Fe^{3+}. These Fe^{3+} ions will replace the Mn^{3+} ions present in the samples. As Mn^{3+} and Fe^{3+} have almost the same ionic radius of 0.645Å [10], little or no change in the lattice parameters by Fe doping is to be expected. On the other hand the bandwidth (W) which is characterized by the overlap between the Mn3d and O2p orbital and which can be described empirically by:

$$W(a.u) \propto \frac{\cos\left[\frac{1}{2}(\pi - \theta_{Mn\text{-}O\text{-}Mn})\right]}{\left(d_{Mn-O}\right)^{3.5}} \text{ [29]} \qquad (2)$$

remains almost independent of iron substitution (298 a.u for x=0.05 and 296 a.u for x=0.2). Consequently lattice effects on magnetic and electrical properties may be ignored in these materials.

3. 2 Magnetic properties

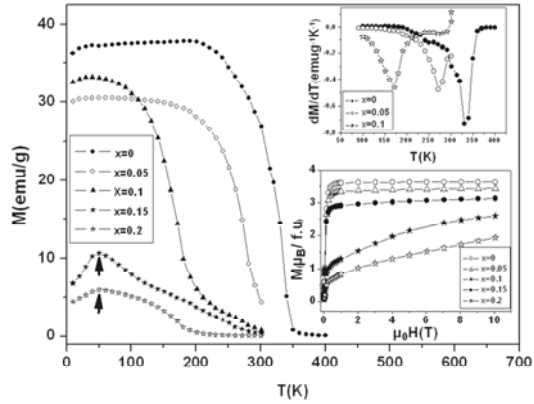

Fig.2. *M (T)* curves for $La_{0.67}Ba_{0.33}Mn_{1-x}Fe_xO_3$ (x = 0- 0.2) at μ_0H= 0.05 T magnetic field in ZFC regime. The arrows indicate spin glass-like at around 50 K for compounds with higher Fe^{3+} concentration. The upper inset is the *dM/dT* curve for x=0 specimen. The lower inset shows *M (H)* curves at 10 K for all specimens.

Fig. 2 presents the temperature dependence of magnetization measurements, *M(T)*, performed for $La_{0.67}Ba_{0.33}Mn_{1-x}Fe_xO_3$ ($0 \leq x \leq 0.2$) samples on heating in a field of 0.05T after cooling without field (ZFC). As shown in Fig. 2, paramagnetic (PM) to ferromagnetic (FM) phase transition is observed at Curie temperature, T_C, below 10% iron concentration. T_C of the samples was determined from peak of $\frac{dM}{dT}$ vs. T representation (the upper inset). T_C value (~332K) for pure sample (x=0), is 18K lower than that earlier reported by Osthöver et al. [11] whose have been investigated low percentage doping of Fe^{3+} ($x \leq 0.1$) in $La_{0.67}Ba_{0.33}Mn_{1-x}Fe_xO_3$ and have shown that T_C decreases from 350K for x=0 to 210K for x = 0.1. Such difference with our results may be due to relatively low temperature annealing (1180°C) if compared with their specimens heating (1400°C). Interestingly, relatively low annealing temperature makes T_C to be near the ambient temperature. For the pure system, the mixed valence can result in strong ferromagnetic interaction arising from the Mn^{3+}-O-Mn^{4+} network, which can be explained by the double exchange interaction mechanism [5-7]. The T_C values extracted from M(T) curves for the samples $0 \leq x \leq 0.1$ are given in table 2. Obviously, substitution of Fe at the Mn- site causes a gradually reduction in Curie temperature. The PM - FM phase transition is relatively sharp for the pure sample, however, in the mixed systems, x = 0.05 - 0.1, the temperature range of PM - FM phase transition becomes broader. This indicates a magnetic inhomogeneity due to a wider distribution of the magnetic exchange interactions Mn^{3+}-O-Mn^{4+} network. Additionally, with increasing Fe- doping level at Mn-site, the magnetic behaviour of the samples with x=0.15 and 0.2 becomes different:

(i) ZFC curves show a sharp cusp of magnetization curves at about 50 K marked by arrow, which can be ascribed to spin-glass-like induced by competing ferromagnetic DE interaction and antiferromagnetic SE interaction [30]. Such cusp is not significant below 10% iron concentration.

(ii) The onset of M(T) curves for x=0.15 and 0.2 specimens show that the PM-FM phase transition was disappeared, so it seems that there is a limit value of iron concentration (x=0.1), in iron doped manganites, which produces such transition.

This is confirmed by our M(H) measurements at 10K (see the lower inset of Fig. 2) which shows that below 10% Fe^{3+} level-doping, the materials exhibit a strong ferromagnetic behaviour, while above that concentration an antiferromagnetic behaviour is predominant for specimens. This behaviour is consistent with early experimental Mössbauer spectroscopy studies [21, 31] which have been shown that the magnetic moments of Fe^{3+} are coupled antiferromagnetically to the ferromagnetic Mn-O lattice. So such disappearance of magnetic transition and hence the establishment of an antiferromagnetic behaviour for high doping concentration should be ascribed to high probability of encountering Fe^{3+}-O-Fe^{3+} antiferromagnetic interaction. The experimental magnetic saturation moment at 10K (M_s^{mes}) for our studies are determined by extrapolating the linear part of high field (10T) magnetization curves to zero field [32]. The observed M_s^{mes} values given in table II are close to those calculated M_s^{calc} according to Eq. 3:

$$M_s^{calc}(\mu_B/f.u) = (0.67-x)M_{Mn^{3+}} + xM_{Fe^{3+}}\cos\alpha + 0.33M_{Mn^{4+}}$$
$$= 2\mu_B\left((0.67-x)\times\frac{4}{2} + x\frac{5}{2}\times\cos\alpha + 0.33\times\frac{3}{2}\right) \quad (3)$$

It seems from the results indicated in table II that the magnetic moments of Fe^{3+} are not completely antiferromagnetically coupled ($\alpha \neq \pi$) to the ferromagnetic Mn-O lattice, so a spin canted state should be established between Fe^{3+} and Mn^{3+}, with an increase in canting angle α when the amount of Fe^{3+} increases. This phenomenon of limiting value of Fe^{3+} amount which destroys the PM-FM transition is consistent with our electrical investigations as discussed in section 3.3.

3.3 Electrical properties

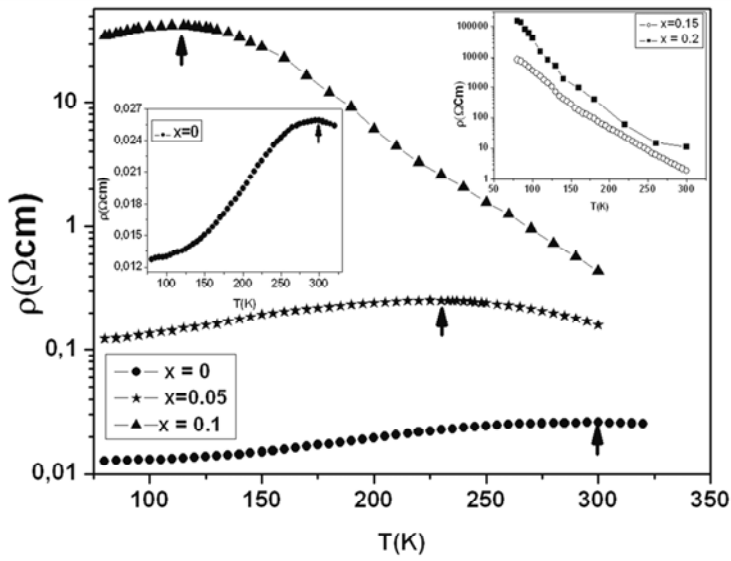

Fig. 3: The temperature dependence of the electrical resistivity ρ *(T)* for $La_{0.67}Ba_{0.33}Mn_{1-x}Fe_xO_3$ (x = 0- 0.2). The arrow indicates metal-semiconductor transition temperature T_P. The left inset is the plot of ρ vs. T in linear scale that clearly shows metal- semiconductor transition for pure sample. The right inset is the plot of ρ vs. T for samples above 10% iron amount showing semiconductor behaviour in all temperature range.

The variation of electrical resistivity with temperature in 80-300K temperature range for x = 0.05- 0.2 doped compounds and in 80-320K temperature range for pure sample is shown in Fig. 3. The samples with $0 \leq x \leq 0.1$ Fe concentrations exhibit a metallic behaviour (i.e. $d\rho/dT > 0$) at low temperature. With rising temperature, metal-semiconductor transition is seen at T_P, indicated by arrow (the left inset shows more clearly the transition for pure sample), where $d\rho/dT < 0$ for a semi conductor behaviour. The maximum resistivity ρ_{max} (peak value) increases and T_P shifts to lower temperature as x increases (see table II). We can see in table II that T_C and T_P follow the same trend indicating coupling of electric and magnetic properties. No metal – semiconductor (MS) transition was observed above x=0.1 Fe amount (see the right inset of Fig 3), so x=0.1 iron

concentration should be the limiting value that destroys the ferromagnetic-metallic (FMM) – paramagnetic- semiconductor (PS) transition in these compounds. This behaviour was encountered in previous works, $Nd_{0.7}Sr_{0.3}Mn_{1-x}Fe_xO_3$ (x = 0 - 0.15) [20] and $La_{0.7}Ca_{0.3}Mn_{1-x}Fe_xO_3$ (x = 0 - 0.12) [33].

Table 2: Curie temperature T_C, experimental and calculated magnetic saturation moments M_S^{mes} and M_S^{cal}, the canting angle α, the peak of resistivity ρ_{max} and the metal – semiconductor transition temperature T_P.

x	T_C(K)	T_P(K)	$\Delta T = T_C - T_P$	M_S^{mes} (μ_B)	M_S^{cal}(μ_B)	α (°)	ρ_{max}(Ωcm)
0	332	297	35	3.61	3.67	-	0.026
0.05	271	230	41	3.44	3.43	100	0.25
0.1	171	114	56	3.12	3.11	108	42
0.15	-	-	-	2.58	2.59	130	-
0.2	-	-	-	1.92	1.93	160	-

The decrease in T_C and T_P with Fe doping in our specimens should be ascribed to the decrease of the ratio Mn^{3+}/Mn^{4+}, which greatly weakens the influence of Mn^{3+}-O-Mn^{4+} DE interactions [21, 34]. The behaviour of the samples can be explained by considering the electronic band structure of the material. The configuration of *d* electrons in transition metal oxides is determined by the internal crystal field. In an octahedral field, the *d* level split into $t_{2g}\uparrow e_g\uparrow$ and $t_{2g}\downarrow e_g\downarrow$. The electronic configuration is $t_{2g}^3 \uparrow e_g^1 \uparrow$, $t_{2g}^3 \uparrow$ and $t_{2g}^3 \uparrow e_g^2 \uparrow$ respectively for Mn^{3+}, Mn^{4+} and Fe^{3+}. Thus the $e_g\uparrow$ band of Mn is electronically active, where electron hopping occurs between Mn^{3+} and Mn^{4+}. Simultaneous existence of Fe^{3+}, Mn^{3+} and Mn^{4+} indicates that the Fe $e_g\uparrow$ band is full and the Mn $e_g \uparrow$ band is half filled. The Fe $e_g\uparrow$ band remains fully filled only if the Mn $e_g \uparrow$ band has charge carriers. This implies that the bottom of the Mn $e_g\uparrow$ band should be at the same level as, or higher than, the top of the Fe $e_g\uparrow$ band. For our materials, there are 0.67-x electrons in Mn $e_g \uparrow$ band, which has a capacity of two electrons, hence the (0.67-x)/2 part of Mn $e_g \uparrow$ band is also filled. So (assuming uniform filling in the band) the highest filled state in Mn $e_g \uparrow$ (Fermi level) will be (0.67-x)/2 eV

above the top of Fe $e_g\uparrow$ band. It is clear from this energy that there are no states on Fe^{3+} which can participate in electron hopping from Mn. Consequently, the doping of Fe results in depletion in the number of hopping electrons and hence weakens the DE interaction, which suppress metallicity and push the system in semiconductor side [28].

4. Conclusion

We have prepared $La_{0.67}Ba_{0.33}Mn_{1-x}Fe_xO_3$ ($0 \leq x \leq 0.2$) manganese oxides by ceramic method at 1180°C. XRD structure analysis and SEM morphological investigation have been shown that the relatively high Fe^{3+} doping - level don't affect both structure parameters and grain sizes of these manganites due to similar ionic radius of Mn^{3+} and Fe^{3+}. Magnetization investigations both with temperature M(T), and with magnetic field M(H), show a (PM) to (FM) phase transition at T_C and with a strong ferromagnetic behaviour at low temperature as shown by M(H) curves for x = 0 - 0.1compounds. No magnetic transition was observed above 10% iron concentration and a spin glass-like was observed at low temperature. For such concentrations M(H) curves clearly show that an antiferromagnetic behaviour is predominant. Electrical properties are very consistent with magnetic ones, particularly the transition from metallic to semi conductor behaviour at T_P occurs for the same concentrations which exhibiting magnetic transition. Interestingly, with the increase in doping concentration, T_C and T_P follow the same trend indicating coupling of electric and magnetic properties. Changes in these properties have been analysed on the basis that the substitution of Fe^{3+} for Mn^{3+} reduces the number of available hopping sites for the Mn $e_g(\uparrow)$ electron and suppresses the double exchange (DE), rather than lattice effect which is insignificant due to similar ionic radii of Fe^{3+} and Mn^{3+}.

References

[1] R. Von Helmolt, J. Wecker, B. Holzapfel, L. Schultz, K. Samwer, Phys. Rev. Lett. **71** (1993) 2333

[2] S. Jin, M. McCormack, T. H. Tiefel, R. Ramesh, J. Appl. Phys. **76** (1994) 6929

[3] F. Bridges, C. H. Booth, G. H. Kwei, J. J. Neumeir, G. A. Swatzky, Phys. Rev. **B 61** (2000) R9237

[4] J. Yang, Y. Q. Ma, R. L. Zhang, B. C. Zhao, R. Ang, W. H. Song, Y. P. Sun, Solid State Commun. **136** (2005) 268

[5] C. Zener, Phys. Rev. **B 82** (1951) 403

[6] P. W. Anderson, H. Hasegawa, Phys. Rev. **100** (1955) 675

[7] P. G. Degennes. Phys. Rev. **118** (1960) 141

[8] A. J. Millis, P. B. Littlewood, B. I. Chairman, Phys. Rev. Lett. **74** (1995) 5144

[9] T. Peterliin-Neumaier, E. Steichele, J. Magn. Magn. Mater. **59** (1986) 351

[10] R. D. Shannon, Acta Crystallogr. **A 32** (1976) 751

[11] C. Osthöver, P. Grünberg, R. R Arnos, J. Magn. Magn. Mater. **177** (1998) 854

[12] S. M. Yusuf, M. Sahana, K. Dorr, U. K. Röbler, K. H. Muller, Phys. Rev. **B 66** (2002) 064414

[13] V. Sen, N. Panwar, G. L. Bahla, S. K Agarwal, J. Phys. Chem. Solids **68** (2007) 1685, J. Alloy. Comp. **439** (2007) 205

[14] L. Li, K. Nishimura, M. Fujii, K. Mori, Solid State Commun. **144** (2007) 10

[15] H. Rahmouni, M. Nouiri, R. Jemai, N. Kallel, F. Rzigua, A. Selmi, K. Khirouni, S. Alaya, J. Magn. Magn. Mater. **316** (2007) 23

[16] K. R. Priolkar, R. Rawat, J. Magn. Magn. Mater. **320** (2008) 325

[17] M. El-Hagary, Y. A. Shoker, S. Mohammad, A. M. Moustapha, A. Abd El-Aal, H. Michor, M. Reissner, G. Hilscher, A. A. Ramadan, J. Alloy. Compd. **468** (2009) 47

[18] X. Wen-Xu, L. Bao-He, Q. Zheng-Nan, J. Han-Min, J. Appl. Phys. 86 (1999) 5164

[19] Q. Huang, Z. W. Li, J. Li, C. K. Ong, J. Appl. Phys. **89** (2001) 7410, J. Phys.: Condens. Matter **13** (2001) 4033

[20] Y. L. Chang, Q. Huang, C. K. Ong, J. Appl. Phys. **91** (2002) 789

[21] A. G. Mostafa, E. K. Abdel-Khalek, W. M. Daoush, S. F. Moustafa, J. Magn. Magn. Mater. **320** (2008) 3356
[22] K. H. Ahn, X. W. Wu, K. Liu, C. L. Chien, Phys. Rev. **B 54** (1996) 15299
[23] L. Righi, P. Gorria, M. Insausti, J.Gutierrez, J. M. Barabdiaran, J. Appl. Phys. **81** (1997) 5767
[24] J. W. Cai, C. Wang, B. G. Shen, J. G. Zhao, W. S. Zhan, Appl. Phys. Lett. **71** (1997) 1727
[25] S. K. Hasanain, M. Madeem, W. H. Sah, M. J. Akhtar, M. M. Hasan, J. Phys.: Condens. Matter **12** (2000) 9007
[26] J. Rodriguez-Carvajal, FULLPROF 2000 –2005, Laboratoire Leon Briouillon (CEA-CNRS)
[27] G. H. Jonker, Physica **20** (1954) 1118
[28] K. H. Ahn, X. W. Wu, K. Liu, C. L. Chien, J. Appl. Phys. **81** (1999) 5505
[29] P. G. Radaelli, G. Iannone, M. Marezio, H. Y. Hwang, S. W. Cheong, J. D. Jorgensen, D. N. Argyriou, Phys. Rev. B **56** (1997) 8265
[30] J. A. Mydosh, *in Spin Glass: An experimental Introduction* (Taylor & Francis, London, 1993)
[31] S. B. Ogale, R. Shreekala, R. Bathe, S. K. Date, S. I. Patil, B. Hannoyer, F. Petit, G. Marest, Phys. Rev. B **57** (1998) 7841
[32] H. Terashita, J. J .Neumeir, Phys. Rev. B **71**, (2005) 134402-1
[33] S. Zemni, A. Gasmi, M. Boudard, M. Oumezzine, Mater. Sc. Eng. B, **144**, (2007), 117
[34] M. S. Sahasrabudhe, S. I. Patil, S. K. Date, K. P. Adhi, S. D. Kulkarni, P. A. Joy, R. N. Bathe, Solid State Commun. **137** (2006) 595
[35] S. Bhattacharya, S. Pal, R. K. Mukherjee, B. K. Chaudhuri, S. Neeleshwar, Y. Y. Chen, S. Mollah, H. D. Yang, J. Magn. Magn. Mater. **269** (2004) 359